ligand-binding extracellular region, which indicates that this domain shows the greatest degree of amino acid diversification and evolves faster than the highly conserved intracellular kinase domain (*29*). The high sequence divergence in the extracellular domain of FER may contribute to reproductive isolation between two species, as has been proposed for other genes involved in recognition at fertilization (*30*).

Our data suggest that FER acts in the filiform apparatus to control the behavior of the pollen tube to achieve fertilization. We propose that the interaction between the putative male ligand and the extracellular domain of the FER RLK triggers a signal transduction cascade inside the synergid cell. A subsequent signal then feeds back from the synergid to the pollen tube, causing growth arrest and the release of the sperm cells. Conceptually, this process is similar to the signaling events occurring during the self-incompatibility reaction in *Brassica* spp. (*31*). In an incompatible pollination, a pollen ligand interacts with a stigma-expressed RLK, inducing a signaling cascade in female papillar cells, which then signal back to the pollen and inhibit its germination. Further studies of the *FER* signaling pathway will help to uncover the molecular mechanism of fertilization and reproductive isolation in plants. Furthermore, the manipulation of the *FER* pathway might allow the generation of hybrids between otherwise incompatible species.

References and Notes

1. M. Hülskamp, K. Schneitz, R. E. Pruitt, *Plant Cell* **7**, 57 (1995).
2. S. M. Ray, S. S. Park, A. Ray, *Development* **124**, 2489 (1997).
3. U. Grossniklaus, K. Schneitz, *Semin. Cell Dev. Biol.* **9**, 227 (1998).
4. T. Higashiyama *et al.*, *Science* **293**, 1480 (2001).
5. R. N. Kapil, A. K. Bhatnagar, *Phytomorphology* **25**, 334 (1975).
6. B. Q. Huang, S. D. Russell, *Int. Rev. Cytol.* **140**, 233 (1992).
7. S. D. Russell, *Int. Rev. Cytol.* **140**, 357 (1992).
8. N. Huck, J. M. Moore, M. Federer, U. Grossniklaus, *Development* **130**, 2149 (2003).
9. N. Rotman *et al.*, *Curr. Biol.* **13**, 432 (2003).
10. C. R. Schopfer, M. E. Nasrallah, J. B. Nasrallah, *Science* **286**, 1697 (1999).
11. M. Mishima *et al.*, *J. Biol. Chem.* **278**, 36389 (2003).
12. S. Kim *et al.*, *Proc. Natl. Acad. Sci. U.S.A.* **100**, 16125 (2003).
13. M. L. Márton, S. Cordts, J. Broadhvest, T. Dresselhaus, *Science* **307**, 573 (2005).
14. W. Tang, D. Kelley, I. Ezcurra, R. Cotter, S. McCormick, *Plant J.* **39**, 343 (2004).
15. K. von Besser, A. C. Frank, M. A. Johnson, D. Preuss, *Development* **133**, 4761 (2006).
16. See supporting material on *Science* Online.
17. S. H. Shiu, A. B. Bleecker, *Plant Physiol.* **132**, 530 (2003).
18. S. H. Shiu, A. B. Bleecker, *Proc. Natl. Acad. Sci. U.S.A.* **98**, 10763 (2001).
19. T. S. Nuhse, A. Stensballe, O. N. Jensen, S. C. Peck, *Plant Cell* **16**, 2394 (2004).
20. P. Primakoff, D. G. Myles, *Science* **296**, 2183 (2002).
21. V. Kaul, J. L. Rouse, E. G. Williams, *Can. J. Bot.* **64**, 282 (1986).
22. E. G. Williams, V. Kaul, J. L. Rouse, B. F. Palser, *Aust. J. Bot.* **34**, 413 (1986).
23. S. J. Hiscock, H. G. Dickinson, *Theor. Appl. Genet.* **86**, 744 (1993).
24. M. K. Kandasamy, J. B. Nasrallah, M. E. Nasrallah, *Development* **120**, 3405 (1994).
25. M. Hülskamp, S. D. Kopczak, T. F. Horejsi, B. K. Kihl, R. E. Pruitt, *Plant J.* **8**, 703 (1995).
26. K. K. Shimizu, K. Okada, *Development* **127**, 4511 (2000).
27. K. K. Shimizu, *Popul. Ecol.* **44**, 221 (2002).
28. M. Nei, T. Gojobori, *Mol. Biol. Evol.* **3**, 418 (1986).
29. S. H. Shiu *et al.*, *Plant Cell* **16**, 1220 (2004).
30. W. J. Swanson, V. D. Vacquier, *Nat. Rev. Genet.* **3**, 137 (2002).
31. A. Kachroo, M. E. Nasrallah, J. B. Nasrallah, *Plant Cell* **14**, S227 (2002).

32. Supported by the University of Zürich, grants from the Swiss National Science Foundation (U.G.) and the National Science Foundation of China (W.-C.Y.), and a Human Frontier Science Program fellowship (S.K.). We thank C. Baroux and P. Barrell for help with confocal analyses; D. Weigel and J.-E. Faure for seeds; M. Curtis, R. Blainvillain, and P. Gallois for plasmids; P. Kopf for technical assistance; and M. A. Collinge and S. E. Schauer for discussions and comments on the manuscript. GenBank accession numbers for *FER* homologs are as follows: *B. oleracea*, EF681131; *A. lyrata*, EF681133; *A. Thaliana* L-*er*, EF681137; *C. flexuosa* 1, EF681134; *C. flexuosa* 2, EF681135; *C. flexuosa* 3, EF681136; *C. flexuosa* 4, EF681132.

Supporting Online Material

www.sciencemag.org/cgi/content/full/317/5838/656/DC1
Materials and Methods
Fig. S1
Table S1
References

9 April 2007; accepted 14 June 2007
10.1126/science.1143562

Quantitative Mass Spectrometry Identifies Insulin Signaling Targets in *C. elegans*

Meng-Qiu Dong,[1] John D. Venable,[1] Nora Au,[2,3] Tao Xu,[1] Sung Kyu Park,[1] Daniel Cociorva,[1] Jeffrey R. Johnson,[1] Andrew Dillin,[2] John R. Yates III[1]*

DAF-2, an insulin receptor–like protein, regulates metabolism, development, and aging in *Caenorhabditis elegans*. In a quantitative proteomic study, we identified 86 proteins that were more or less abundant in long-lived *daf-2* mutant worms than in wild-type worms. Genetic studies on a subset of these proteins indicated that they act in one or more processes regulated by DAF-2, including entry into the dauer developmental stage and aging. In particular, we discovered a compensatory mechanism activated in response to reduced DAF-2 signaling, which involves the protein phosphatase calcineurin.

The insulin signaling pathway and insulin-like growth factor–1 (IGF-1) signaling pathway are conserved from invertebrates to mammals (*1*, *2*). DAF-2, the sole homolog of the insulin receptor or IGF-1 receptor in *C. elegans*, controls the expression of presumably a large number of downstream targets by negatively regulating DAF-16, a FoxO transcription factor (*3*–*8*). In this study, we integrated technological advancements in quantitative mass spectrometry (MS) (*9*–*11*), including labeling multicellular organisms with the ^{15}N stable isotope, to identify DAF-2 signaling targets. We made direct measurements of proteins as opposed to mRNAs, which are not final gene products. Our method allows for the identification of targets not regulated at the transcription level. The MS techniques demonstrated in this study can be readily used to determine protein abundance changes as a result of genetic or pharmacological perturbations.

[1]Scripps Research Institute, La Jolla, CA 92037, USA. [2]Salk Institute for Biological Studies, La Jolla, CA 92037, USA. [3]University of California at San Diego, La Jolla, CA 92093, USA.

*To whom correspondence should be addressed. E-mail: jyates@scripps.edu

We prepared lysates from wild-type (WT), *daf-16(mu86)* null, or *daf-2(e1370ts)* worms in their first day of adulthood, a period important for regulation of longevity by DAF-2 signaling (*8*). These lysate samples were mixed at a 1:1 ratio with a reference sample in which all proteins were labeled with ^{15}N (atomic enrichment of $^{15}N \geq 96\%$) [(*12*) and fig. S1]. This reference sample was a lysate of WT worms fed with bacteria that were grown in a medium enriched in ^{15}N. Soluble proteins (S100 fraction) from the lysate mixtures were then digested and analyzed by MS. A total of 1685 proteins were identified. Using its ^{15}N-labeled counterpart as a reference, we determined the relative abundance of each unlabeled (i.e., ^{14}N-labeled) protein with a modified version of the RelEx software (*10*). We also assessed the relative abundance of individual proteins by spectral counting (SC), in which we counted how many times the unlabeled version of a protein was identified by the fragmentation spectra of its peptides. Spectral counts correlate with protein abundance (*11*). We detected little difference between the *daf-16* and WT samples (fig. S2A), reflecting the fact that *daf-16* and WT adult worms were phenotypically similar under our experimental conditions (*3*, *4*, *6*–*8*). In contrast, we observed many protein abundance changes in the *daf-2* mutants as compared with those in WT worms (fig. S2B), with an obvious correlation (i) between the RelEx and SC measurements ($r = 0.59$) and (ii) between the

two *daf-2* samples (r = 0.83, fig. S3). Using stringent criteria that emphasize high-quality measurements and consistent changes (table S1), we identified 86 proteins that were differentially expressed in the S100 fraction of the *daf-2* sample (tables S2 and S3). Of these proteins, 47 were more abundant and 39 were less abundant than those in the WT sample. A subset of these proteins corresponds to known DAF-16 target genes, including superoxide dismutase *sod-3* (*7*, *13*).

To assess the quality of the quantitative MS results, we used selected reaction monitoring (SRM) to validate a subset of these results. For SRM, we measured the intensity of a specific fragment ion from a specific precursor ion (*12*). SRM is suitable for monitoring selected peptides at multiple time points. We reasoned that if a protein is truly regulated in *daf-2* mutants, then the difference in its abundance between the WT and the *daf-2* mutant animals should increase gradually during the temperature shift from 15°C (permissive for *e1370*) to 20°C (semi-permissive) and 25°C (nonpermissive). This was indeed the case with the three proteins that we monitored (Fig. 1, A to C). Western blotting results also correlated directly with MS results for nine proteins tested (Fig. 1, D to L, and fig. S4). Thus, the SRM and Western blotting results confirmed the accuracy of the quantitative proteomic results.

Other researchers have previously identified DAF-16 target genes that barely overlapped between studies (*13*–*16*). To help clarify this issue, we compared results (tables S2 and S3) and found that ours matched best with a microarray analysis by Murphy *et al*. (*13*). In total, only 35 proteins identified in this study were identified in previous studies (tables S2 and S3). The remaining 51 proteins may be previously unrecognized targets of the DAF-2 signaling pathway.

To understand the protein abundance changes in the context of protein function, we adopted GoMiner software (*17*) to classify the differentially expressed proteins on the basis of their annotation in the gene ontology database (table S2). Proteins whose abundance decreased in *daf-2* mutant animals were enriched for functions in translation elongation and lipid transport. In contrast, proteins that became more abundant in *daf-2* mutant animals were enriched for functions in amino acid biosynthesis, oxygen and reactive oxygen species metabolism, and carbohydrate metabolism [including gluconeogenesis and the glyoxylate cycle (GC), a modified version of the tricarboxylic acid cycle].

To determine whether the signaling targets identified in this study function in DAF-2–dependent processes such as dauer formation, we used RNA interference (RNAi) to analyze a subset of these targets (Fig. 2A). We found that *npa-1* RNAi suppressed dauer formation in *daf-2* mutants as strongly as did *daf-16* RNAi. *npa-1* encodes a polyprotein precursor for multiple fatty acid–binding and retinol-binding proteins (www.wormbase.org). This result suggests that NPA-1, which has increased abundance in the *daf-2* mutant (tables S2 and S3), plays a critical role in dauer formation. Several genes functioning in carbohydrate metabolism also seem to be important for *daf-2* dauer formation (Fig. 2A).

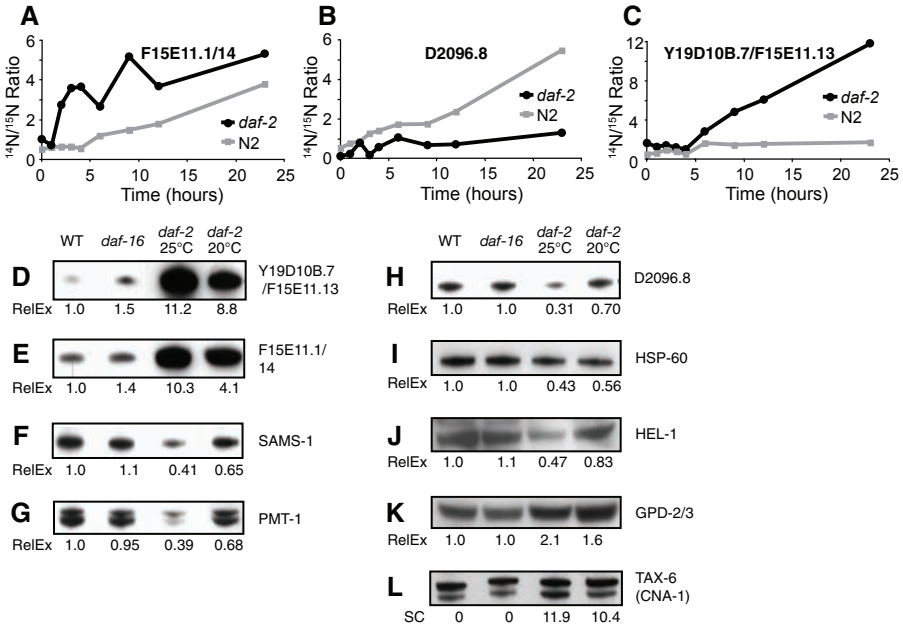

Fig. 1. Confirmation of quantitative proteomic results by SRM and Western blotting. (**A** to **C**) SRM quantitation of the abundance of F15E11.1/14, D2096.8, and Y19D10B.7/F15E11.13 in WT (N2) and *daf-2* mutant animals after a temperature shift from 15° to 20°C for 3 hours and then to 25°C for 20 hours. Samples were collected (at times indicated), lysed, and mixed at a 1:1 ratio with a ^{15}N-labeled standard derived from WT worms. The S100 fractions were analyzed. (**D** to **L**) The amounts of nine proteins in the S100 fraction of WT, *daf-16(mu86)*, or *daf-2(e1370ts)* worms were visualized by Western blotting. Shown below the blot of each protein is the relative abundance of that protein normalized to the WT amount as determined by RelEx with the use of a ^{15}N-labeled standard [(D) to (K)] or by normalized SC (L).

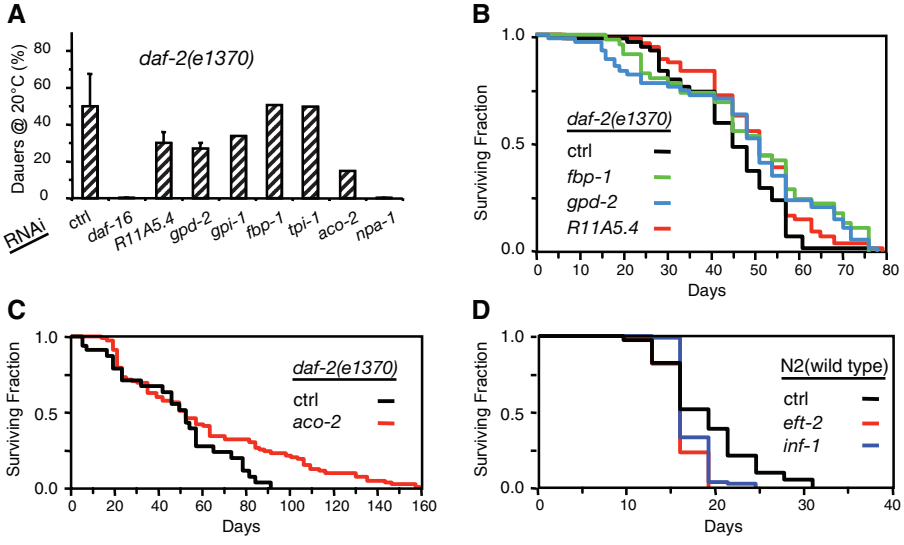

Fig. 2. Function of a subset of the identified DAF-2 signaling targets in life-span regulation, dauer formation, or both. (**A**) Suppression of dauer formation of *daf-2(e1370ts)* animals by RNAi of *npa-1* and several genes involved in carbohydrate metabolism. Percentages of dauers were averaged from four (for Ctrl, *daf-16*, *R11A5.4*, and *gpd-2* RNAi) or two (for RNAi of the remaining genes) independent experiments (n > 110 animals in each experiment). Error bars indicate SE. Ctrl, control. (**B** and **C**) Effects of *fbp-1*, *gpd-2*, *R11A5.4*, and *aco-2* RNAi on the life span of *daf-2(e1370)* mutant animals (one experiment, $n \geq 39$ animals). (**D**) Effects of RNAi of *inf-1*, a translation initiation factor, and *eft-2*, an elongation factor, on the life span of WT worms (one experiment, $n \geq 80$ animals). All P values are less than 0.05 (log-rank tests) between sample and control.

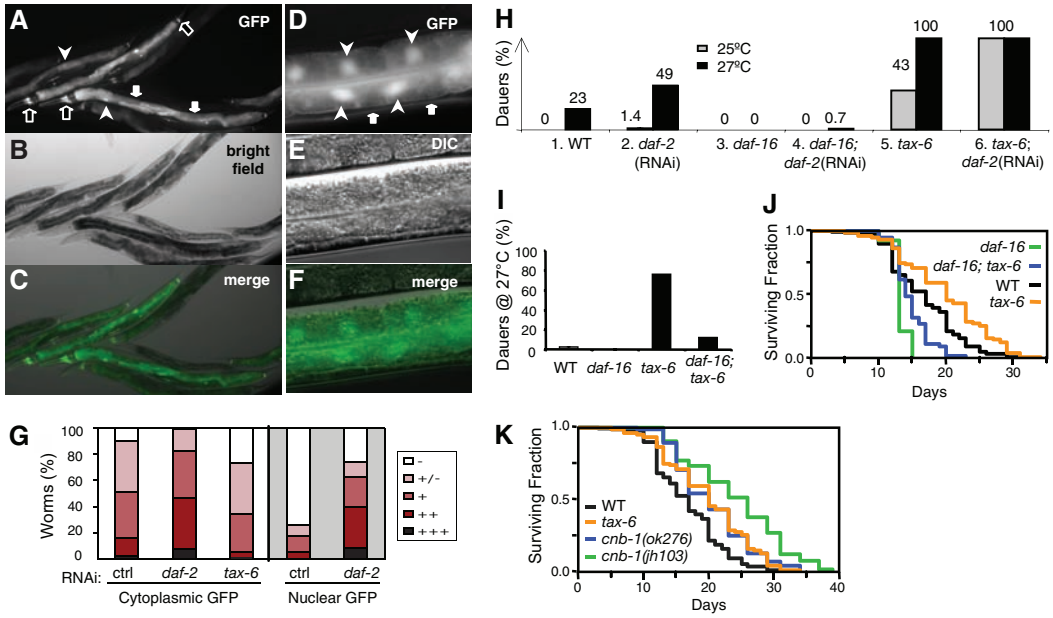

Fig. 3. Identification of TAX-6 as a target and a positive regulator of DAF-2 signaling. (**A** to **F**) TAX-6::GFP was expressed in neurons (open arrows) and in the cytoplasm (solid arrows) and nucleus (arrowheads) of intestinal cells. *tax-6(p675); Ex[pAK13]* animals were imaged at magnifications 100× [(A) to (C)] and 400× [(D) to (F)]. DIC, differential interference contrast. (**G**) Expression of TAX-6::GFP in the intestine of animals treated with control, *daf-2*, or *tax-6* RNAi. The intensity of cytoplasmic and nuclear TAX-6::GFP in the intestine was scored separately. Percentages of worms expressing strong (+++), intermediate (++), weak (+), very weak (+/–), or background (–) TAX-6::GFP in the intestine were averaged from three experiments ($n \geq 39$ animals in each experiment). (**H**) Effects of the *tax-6(p675)* mutation on dauer formation and a synthetic effect with *daf-2* RNAi. WT ("1" and "2"), *daf-16 (mu86)* ("3" and "4"), and *tax-6(p675)* ("5" and "6") animals were treated with *daf-2* ("2," "4," and "6") or control RNAi ("1," "3," and "5") at 27°C (black, one experiment) or 25°C (gray, average of two experiments) ($n > 120$ animals in each experiment). (**I**) *daf-16(mu86)* suppressed *tax-6(p675)* dauer formation (average of two experiments, $n > 300$ animals per experiment). (**J**) *daf-16(mu86)* suppressed the long life span of *tax-6(p675)* mutant animals (one experiment, $n \geq 80$ animals, $P < 0.01$, log-rank test). (**K**) *cnb-1* mutants displayed an extended life span (one experiment, $n \geq 80$ animals, $P < 0.01$, log-rank test).

Given the importance of insulin signaling and IGF-1 signaling in aging, we asked whether these targets play a role in life-span regulation, and we focused on a subset of proteins involved in gluconeogenesis, GC, or translation. RNAi of some of the genes that we tested showed no significant effect on life span (table S4). However, RNAi of *R11A5.4* (phosphoenolpyruvate carboxykinase), *fbp-1* (fructose bisphosphatase), *gpd-2* (glyceraldehyde-3-phosphate dehydrogenase), and *aco-2* (aconitase) further extended the life span of *daf-2* mutants ($P < 0.05$, log-rank test) (Fig. 2, B and C) and so did RNAi of *gpi-1* (glucose phosphate isomerase) (*18*). RNAi of *eft-2* (an elongation factor) or *inf-1* (an initiation factor) shortened the life span of WT worms ($P < 0.05$, log-rank test) (Fig. 2D). Because R11A5.4, FBP-1, GPD-2, ACO-2, and GPI-1 showed increased abundance in the *daf-2* mutant, whereas EFT-2 and INF-1 showed decreased abundance (table S2), these results suggest that abundance changes of proteins involved in carbohydrate metabolism or translation do not necessarily contribute to the longevity of *daf-2* mutants. Instead, such changes may reflect a compensatory mechanism or mechanisms activated by a reduction in DAF-2 signaling.

Another protein exemplifying a compensatory mechanism is TAX-6 or CNA-1, the *C. elegans* calcineurin A protein that is the catalytic subunit of a serine or threonine protein phosphatase. The activity of calcineurin A requires the regulatory subunit calcineurin B (CNB-1 in *C. elegans*) (*19*). TAX-6 and CNB-1 are expressed in multiple cell types (*20*, *21*) including intestinal epithelial cells (Fig. 3, A to F), a site of action for DAF-16 (*22*). Neither *tax-6* nor *cnb-1* has been implicated in the DAF-2 signaling pathway. Both genes lack the DAF-16 binding element (*13*) in a 1.5-kb region upstream of the start codon.

Our MS result indicated a higher TAX-6 abundance in *daf-2* mutant worms as compared to WT worms (table S2). This was verified by Western blotting (Fig. 1L) and by comparing the green fluorescent protein (GFP) signal in animals expressing a TAX-6::GFP fusion protein (Fig. 3G) (*20*). When these worms were treated with *daf-2* RNAi, cytoplasmic as well as nuclear TAX-6::GFP increased in intestinal cells.

Both *tax-6* and *cnb-1* loss-of-function mutants displayed phenotypes that were similar to but weaker than those of *daf-2* mutants, such as an extended life span and increased propensity to entering the dauer phase (Fig. 3, H to K, fig. S5, and table S4). *tax-6(p675)* acted synergistically with *daf-2(RNAi)* (Fig. 3H), and *daf-16(mu86)* partially suppressed *tax-6(p675)* (Fig. 3, I and J). Thus, the TAX-6 and CNB-1 complex (i) facilitates DAF-2 signaling in life-span regulation and dauer formation and (ii) acts in parallel to DAF-16 or acts both upstream of and in parallel to DAF-16. Further epistasis analysis suggested that *tax-6* acts upstream of or in parallel to *age-1*, which encodes a phosphatidylinositol 3-kinase downstream of *daf-2* (see supporting online material text).

Although TAX-6 facilitates DAF-2 signaling, TAX-6 itself is regulated by DAF-2 because reduced DAF-2 signaling results in increased abundance of TAX-6. Thus, TAX-6 is part of a feedback loop that acts to maintain DAF-2 signaling at normal levels. This again suggests a compensatory mechanism. We propose that the life span of *daf-2* mutants results from two types of changes: One change extends life span (e.g., SOD-3) and the other, represented by the compensatory mechanism(s) involving TAX-6 and several proteins functioning in carbohydrate metabolism or translation, shortens life span. Thus, inhibition of the compensatory mechanism can further extend the life span of *daf-2* mutants (e.g., by *aco-2* RNAi). Further investigation of the compensatory mechanism and DAF-2 signaling targets identified here is likely to aid the research of diabetes and aging in mammals.

References and Notes

1. A. R. Saltiel, C. R. Kahn, *Nature* **414**, 799 (2001).
2. M. F. White, *Am. J. Physiol. Endocrinol. Metab.* **283**, E413 (2002).
3. C. Kenyon, J. Chang, E. Gensch, A. Rudner, R. Tabtiang, *Nature* **366**, 461 (1993).
4. K. D. Kimura, H. A. Tissenbaum, Y. Liu, G. Ruvkun, *Science* **277**, 942 (1997).
5. S. Ogg *et al.*, *Nature* **389**, 994 (1997).
6. D. Gems *et al.*, *Genetics* **150**, 129 (1998).
7. Y. Honda, S. Honda, *FASEB J.* **13**, 1385 (1999).
8. A. Dillin, D. K. Crawford, C. Kenyon, *Science* **298**, 830 (2002).
9. J. Krijgsveld *et al.*, *Nat. Biotechnol.* **21**, 927 (2003).
10. J. D. Venable, M. Q. Dong, J. Wohlschlegel, A. Dillin, J. R. Yates III, *Nat. Methods* **1**, 39 (2004).
11. H. Liu, R. G. Sadygov, J. R. Yates III, *Anal. Chem.* **76**, 4193 (2004).
12. Materials and methods are available as supporting material on *Science* Online.
13. C. T. Murphy *et al.*, *Nature* **424**, 277 (2003).
14. J. J. McElwee, E. Schuster, E. Blanc, J. Thornton, D. Gems, *Mech. Ageing Dev.* **127**, 458 (2006).
15. S. S. Lee, S. Kennedy, A. C. Tolonen, G. Ruvkun, *Science* **300**, 644 (2003).
16. S. W. Oh *et al.*, *Nat. Genet.* **38**, 251 (2006).
17. B. R. Zeeberg *et al.*, *Genome Biol.* **4**, R28 (2003).

18. M. Hansen, A. L. Hsu, A. Dillin, C. Kenyon, *PLoS Genet.* **1**, 119 (2005).
19. J. Lee *et al.*, *J. Mol. Biol.* **344**, 585 (2004).
20. A. Kuhara, H. Inada, I. Katsura, I. Mori, *Neuron* **33**, 751 (2002).
21. J. Bandyopadhyay *et al.*, *Mol. Biol. Cell* **13**, 3281 (2002).
22. N. Libina, J. R. Berman, C. Kenyon, *Cell* **115**, 489 (2003).
23. We thank WormBase (www.wormbase.org); the *Caenorhabditis* Genetics Center; A. Kuhara, I. Mori, I. Katsura, J. Ahnn, and T. Blumenthal for databases and reagents; and M. Koelle, L.-L. Du, A. Aslanian, I. Cheeseman, and members of the Yates and Dillin laboratories for help with the manuscript, experiments, and grant applications. M. MacCoss and C. Wu helped determine the atomic enrichment of ^{15}N in labeled worms. J.V. was supported by a NIH National Research Service Award fellowship. This work was supported by NIH grants DK067598, DK074798, DK070696, and P41 RR11823-10.

Supporting Online Material
www.sciencemag.org/cgi/content/full/317/5838/660/DC1
Materials and Methods
SOM Text
Figs. S1 to S5
Tables S1 to S4
References

16 January 2007; accepted 12 June 2007
10.1126/science.1139952

Forced Unfolding of Proteins Within Cells

Colin P. Johnson,[1]*†‡ Hsin-Yao Tang,[2]* Christine Carag,[1]†‡ David W. Speicher,[2]† Dennis E. Discher[1,2]†‡¶

To identify cytoskeletal proteins that change conformation or assembly within stressed cells, in situ labeling of sterically shielded cysteines with fluorophores was analyzed by fluorescence imaging, quantitative mass spectrometry, and sequential two-dye labeling. Within red blood cells, shotgun labeling showed that shielded cysteines in the two isoforms of the cytoskeletal protein spectrin were increasingly labeled as a function of shear stress and time, indicative of forced unfolding of specific domains. Within mesenchymal stem cells—as a prototypical adherent cell—nonmuscle myosin IIA and vimentin are just two of the cytoskeletal proteins identified that show differential labeling in tensed versus drug-relaxed cells. Cysteine labeling of proteins within live cells can thus be used to fluorescently map out sites of molecular-scale deformation, and the results also suggest means to colocalize signaling events such as phosphorylation with forced unfolding.

Force-induced changes in protein conformation have long been postulated to contribute to the deformability of cells (*1*, *2*). Likewise, in cell adhesion, forces of pico-Newton magnitude that result from cells pulling on matrix (*3*) are believed to induce conformational changes that initiate essential anchorage signals (*4*–*8*). Single-molecule measurements indeed show that domain unfolding occurs in reversible extension of purified cytoskeletal, motor, and matrix adhesion proteins (*9*–*12*), and simulations of the molecular dynamics of protein extension have helped to clarify mechanisms (*13*–*15*). Direct cell-level evidence is lacking or even contrary to forced unfolding (*16*), although cytoskeletal association of a large and rare conformation-sensitive antibody has suggested extension of a proline-rich region in one protein within spread, fixed cells (*17*). The more broadly directed "shotgun" approach here is applied to live cells under physiological stresses and exploits small thiol-reactive probes that permanently label force-sensitive domains.

Cysteine (Cys) is a moderately hydrophobic amino acid that is frequently shielded by tertiary or quaternary protein structure. Labeling of cysteine's SH moiety has been exploited in solution denaturation studies on a few small purified proteins (*18*, *19*), as well as in an anemia-causing proline mutation in the red blood cell (RBC) protein spectrin (*20*). In addition, forced unfolding of single proteins with core-sequestered disulfides demonstrates reduction of the S-S within seconds by reactive thiols in the medium (*21*, *22*). We show here, in intact cells, that force-induced changes in protein structure can also expose—for relatively rapid reaction—specific buried Cys (Fig. 1) in a number of key cytoskeletal proteins. Sequential *n*-dye–labeling with different color fluorophores ($n = 2$ here) proves to be a facile approach to amplifying signals from shielded sites relative to prelabeled surface sites (*23*). We illustrate the range of this in situ "Cys shotgun" approach, first, with the relatively simple human RBC, which allows for the most direct demonstration of forced unfolding in fluid-stressed cells, then, with human mesenchymal stem cells (MSCs) under cell-generated tension.

Red blood cells deform under the incessant stresses of blood flow, and the spectrin membrane cytoskeleton has proven central to cell deformability (*24*). Spectrin's α and β chains interact to cross-link F-actin in this cell, and in single-molecule studies, spectrin's tandem array of helical bundle domains (Fig. 1) are found to unfold at low forces [~picoNewton (*25*–*27*)] that could be generated by just a few myosin motor molecules. There are 20 Cys in α-spectrin and 15 Cys in β-spectrin, and some of these appear buried in crystal structures (Fig. 1) and homology models. To assess exposure of Cys in unfolding of spectrin and all of the other RBC membrane proteins, cells were reversibly lysed to make hemoglobin-depleted pink "ghosts" that were resealed with entrapment of the Cys-reactive fluorophore IAEDANS. Dye-loaded cells were then either held static in suspension at various temperatures or else sheared over a physiological range of stresses with a standard fluid shearing device. After 5 min or more, cells were relysed, excess dye was quenched, and cells were imaged to assess membrane labeling (Fig. 2A).

Solubilized cells were denatured, and all Cys that were not dye-labeled were alkylated with iodoacetamide (IAM). Separation of membrane proteins by one-dimensional (1D) SDS–polyacrylamide gel electrophoresis (SDS-PAGE), followed by densitometry, showed 50% more IAEDANS fluorescence in the bands of α- and β-spectrin from the shear samples (Fig. 2A: 15 runs at 37°C); sequential two-dye labeling magnifies this difference to >500%, as described below. Labeling under shear is only enhanced for spectrin: Labeling of the other major membrane proteins (ankyrin, protein 4.1, actin, etc.)

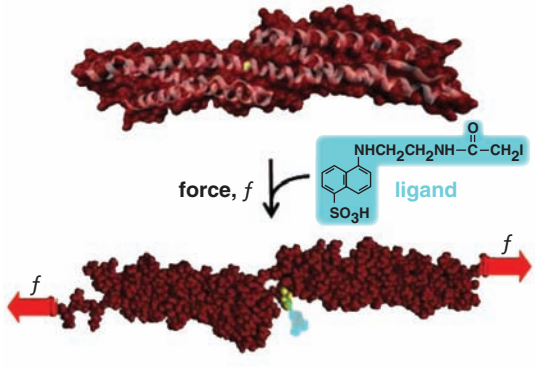

Fig. 1. Force-induced changes in protein structure within cells are hypothesized to expose novel binding sites for ligands. This example of a molecular dynamics simulation shows that Cys^{1167} in β-spectrin exposes 0 $Å^2$ surface area (of 224 $Å^2$) until forced extension [e.g., (*15*)] exposes the -SH for reaction with a thiol-reactive fluorescent dye.

[1]Biophysical Engineering Lab, University of Pennsylvania, Philadelphia, PA 19104, USA. [2]Systems Biology Division—The Wistar Institute, Philadelphia, PA 19104, USA.

*These authors conducted experiments.
†These authors designed, refined, and analyzed experiments.
‡These authors modeled the data and wrote the paper.
¶To whom correspondence should be addressed. E-mail: discher@seas.upenn.edu